Journal of Southeast University (English Edition) Vol. 40, No. 3, pp. 266 – 274 Sept. 2024 ISSN 1003—7985

Influence of the boundary effect on the mechanical response test of pavement cushion under the wetting effect of silt

Luo Qiqi[1] Yu Qian[2] Zhang Sheng[1] Ma Xinyan[1,2] Ye Xinyu[1,3] Du Yinfei[1,3]

([1]School of Civil Engineering, Central South University, Changsha 410075, China)
([2]Department of Geotechnical Engineering, China Airport Planning and Design Institute Co., Ltd., Beijing 100020, China)
([3]Hunan Tieyuan Civil Engineering Testing Co., Ltd., Changsha 410075, China)

Abstract: Through a self-developed model test system, the mechanical properties of silt and the deformation characteristics of airport runways were investigated during the period of subgrade wetting. Based on the test results, the reliability of the numerical simulation results was verified. Numerical models with different sizes were established. Under the same cushion parameter and loading width ranges, the effects of the cushion parameters and loading conditions on the mechanical responses of the cushion before and after subgrade wetting were analyzed. The results show that the internal friction angles of silt with different wetting degrees are approximately 34°. The cohesion is from 8 to 44 kPa, and the elastic modulus is from 15 to 34 MPa. Before and after subgrade wetting, the variation rates of the cushion horizontal tensile stresses with the same cushion parameters and loading width ranges are different under the influence of boundary effects. After subgrade wetting, the difference in the variation rates of the cushion horizontal tensile stresses under the same cushion parameter range decreases compared with that before subgrade wetting; however, this difference increases under the same loading width range. Before and after subgrade wetting, the influence of the boundary effect on the mechanical response evaluation of the cushion is not beneficial for optimizing the pavement design parameters. When the cushion thickness is more than 0.25 m, the influence of the boundary effect can be disregarded.

Key words: pavement cushion; silt subgrade; wetting; boundary effect; mechanical response

DOI: 10.3969/j.issn.1003 – 7985.2024.03.006

The pavement cushion, which is a critical layer of pavement structure, significantly influences the service performance of the subgrade under aircraft loading[1–3]. The mechanical properties of the filling silt of the airport runway are considerably affected by water content[4–6]. During airport loading, the localized wetting problem often occurs in the shallow silt subgrade[7–8]. The stress state of the cushion is largely affected by the uneven deformation of the silt subgrade because of subgrade wetting, which ultimately leads to pavement damage[3,9–10]. Thus, the analysis of the stress behavior of the cushion with different cushion parameters under the influence of subgrade wetting is relevant.

Field[11–12] and laboratory[13–16] tests were adopted to assess the stress behavior of the pavement structure caused by traffic loads. The influence of different composite materials, temperatures, loading amplitudes, and loading frequencies on the bottom strain of asphalt pavement layers was examined through field investigation[17]. Meanwhile, a prediction model for calculating the accumulated strain was proposed. Zhang[18] analyzed the influence of the pavement parameters, loading conditions, and contact states between pavement layers on the pavement strain and determined the evolution characteristics of pavement strain. In summary, the field test is costly, and many complicated factors are uncontrollable. However, the boundary effect of the model needs to be considered for the laboratory test.

Previous studies have shown that the influence of the boundary effect on laboratory experiments cannot be disregarded. For the upper hard and lower soft subgrade layers, Cao et al.[19] provided a formula for calculating the dynamic stress attenuation of the subgrade with different model sizes, and the reliability of the calculation formula was verified in engineering practice. Kuo et al.[20] investigated the mechanical response of the pavement caused by a falling hammer in roadbed compaction tests with different model sizes and identified the appropriate model size. The aforementioned studies indicate that the model size is the main evaluation factor of the boundary effect, but their findings regarding the boundary effect overlooked the influence of water. Meanwhile, under the influence of the water, the applicability of their conclusions regarding the boundary effect still needs to be further proven.

In actual airport engineering, the wetting problem of

Received 2023-12-03, **Revised** 2024-04-02.

Biographies: Luo Qiqi (1992—), male, Ph. D. candidate; Ye Xinyu (corresponding author), male, doctor, associate professor, yexinyu113@csu.edu.cn.

Foundation items: The National Natural Science Foundation of China (No. 52008401), the Natural Science Foundation of Hunan Province (No. 2021JJ40770), the Open Fund of Hunan Tieyuan Civil Engineering Testing Co., Ltd. (No. HNTY2022K04).

Citation: Luo Qiqi, Yu Qian, Zhang Sheng, et al. Influence of the boundary effect on the mechanical response test of pavement cushion under the wetting effect of silt[J]. Journal of Southeast University (English Edition), 2024, 40(3): 266 – 274. DOI: 10.3969/j.issn.1003 – 7985.2024.03.006.

the subgrade occurs frequently[21-22]. Under the influence of the boundary effect of a model test, quantitative analysis of the stress behavior of the cushion induced by aircraft loading and subgrade wetting is still lacking. Thus, this study conducted a mechanical response test for wetting silt subgrade, and the deformation development trends of the cushion caused by subgrade wetting were determined. A validated numerical model was also established to analyze the influence of the boundary effect on the stress behavior of the cushion with subgrade wetting. The results can provide recommendations for avoiding the boundary effects and selecting size in similar subgrade model tests.

1 Experimental Procedures

1.1 Model test design

Based on the specifications of the airport runway design[23], the actual size of a single slab and the wheel distribution of an A380 aircraft were selected in the design of the model test. Under wetting conditions of the silt subgrade, to assess the impact of the boundary effect on the mechanical behavior of the cushion induced by aircraft loading, a loading test device was manufactured and reported in Ref. [24]. The sizes of the physical model box are 2.0, 2.0, and 1.8 m. The sensors embedded in the physical model include the settlement and volumetric water content sensors.

1.2 Materials

The runway in the model test was composed of the cushion and the subgrade. The particle grading curve of the cushion and the silt material have been reported in Ref. [24]. The optimized water content and maximum dry density of the silt sample are 16% and 1 890 kg/m^3, respectively. From the code for airport runway design[24], a compaction degree of 95% was selected, and the thicknesses of the cushion and subgrade were 0.15 and 1.45 m, respectively. The materials used in the model test were fully consistent with the actual engineering materials, and the thickness of the cushion was the same as that in the real case. The physical model test results were used to verify the behavior of the cushion and subgrade under loading in the numerical model; thus, the similarity principle is not considered. To avoid the uneven compaction problem during sample preparation and moisture change in the soil mixing process, the compaction degree of the silt material in layers was checked.

1.3 Experimental scheme

Given the interaction between the adjacent pavement slabs and the largest uneven loading condition, the stress distributions of Slab No. 2 and No. 6 (with high stiffness) in Ref. [24] were selected as the loading conditions. From the specifications[25], the breadth of the concrete slab exceeds four times the thickness of the base course. Thus, the stress diffusion effect during stress transmission in the pavement layers is not considered. The stresses of Slab No. 2 and No. 6 transferred to the cushion surface are 99.03 and 29.62 kPa, respectively. Six wetting processes were conducted in the model test[24], and the injection volume of the water remained unchanged during every single wetting process.

2 Verification of the Numerical Model

2.1 Direct shear and consolidation tests of the wetting silt sample

To establish a numerical model corresponding to the model test, the basic parameters of the wetting silt sample need to be determined. This section mainly introduces the direct shear and consolidation tests of the silt samples with various wetting degrees. The relationship between the compressive modulus (E_s) and the elastic modulus (E) is expressed as follows:

$$E = E_s\left(1 - \frac{2\mu^2}{1-\mu}\right) \tag{1}$$

where μ is the Poisson's ratio. The silt sample has been presented in Ref. [24].

The evolution characteristics of the deformation and strength parameters are listed in Tables 1 and 2, respectively. The elastic modulus and cohesion of silt have a quadratic function relationship with the degree of saturation. The cohesion is from 8 to 44 kPa, and the elastic modulus is from 15 to 34 MPa. The wetting degree of the silt material has limited influence on the internal friction angle, and it remains at approximately 34°.

Table 1 Deformation parameters of silt with different degrees of saturation

Degree of saturation/%	42	54	70	86	97
Elastic modulus/MPa	28	34	32	19	15

Table 2 Strength parameters of silt with different degrees of saturation

Degree of saturation/%	43	55	65	76	87	98
Cohesive/kPa	24	44	38	15	8	5
Friction angle/ (°)	33	36	30	29	36	35

2.2 Introduction and verification of the numerical model

2.2.1 Distribution of the water field of the silt subgrade

The evolution characteristics of the water field of the silt subgrade have been discussed in Ref. [24]. The silt is close to a saturated state at the bottom of the subgrade during the process of the entire test. The degree of saturation at the shallow part of the subgrade shows an increasing trend until it increases to the same value as that at the

middle of the subgrade. The silt at the bottom of the subgrade gradually reaches a saturated state. The analysis indicates that silt has a poor water retention capability and a strong water sensitivity.

2.2.2 Verification of the numerical model

The ABAQUS numerical analysis software was chosen to establish the numerical model. The cushion and silt subgrade were simulated by a 3D solid element, and the grid of the loading area is locally densified. The Mohr-Colomb model was chosen as the constitutive model. The deformations on the side and bottom of the numerical model were constrained. The composition and size of the numerical model are shown in Fig. 1. The numerical model was completely consistent with the model test. Aircraft static loading was applied in the numerical model. According to the water field of the silt subgrade and the basic mechanical parameters of the silt material with various wetting degrees, the parameters of the silt material were assigned to the subgrade at various depths. The other parameters of the numerical model are listed in Table 3.

Table 3 Basic parameters corresponding to the numerical model

Part	Dry density/(kg · m^{-3})	Cohesive/kPa	Internal friction angle/(°)	Elastic modulus/MPa	Poisson's ratio	Void ratio
Cushion	2 000			180	0.25	0.30
Subgrade	1 800	48.6	28.8	32	0.35	0.35

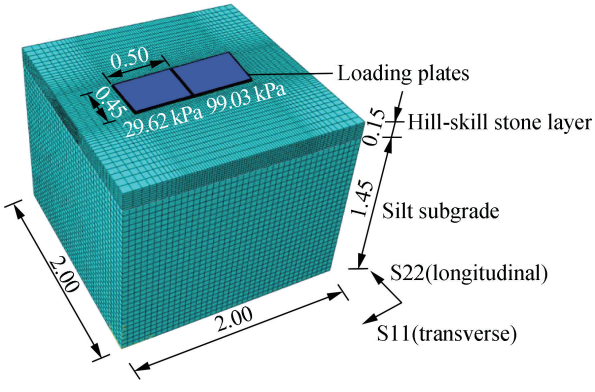

Fig. 1 Wetting numerical model of the airport runway corresponding to the experiment(unit:m)

Fig. 2 shows the evolution characteristics of the uneven vertical deformation between measurement points during the wetting process. The uneven vertical deformation under loading gradually increases after a rapid increase as the wetting time increases. The uneven vertical deformation between measuring points shows a gradually increasing trend as the wetting time increases. During the wetting process, the setting of the cushion increases the inhomogeneous deformation of the runway under loading but significantly decreases the inhomogeneous plastic deformation of the runway. The evolution characteristics of the numerical and experimental results are the same. Most of the simulated values match the experimental results, which indicates that the numerical model can exhibit stress and deformation responses in real cases.

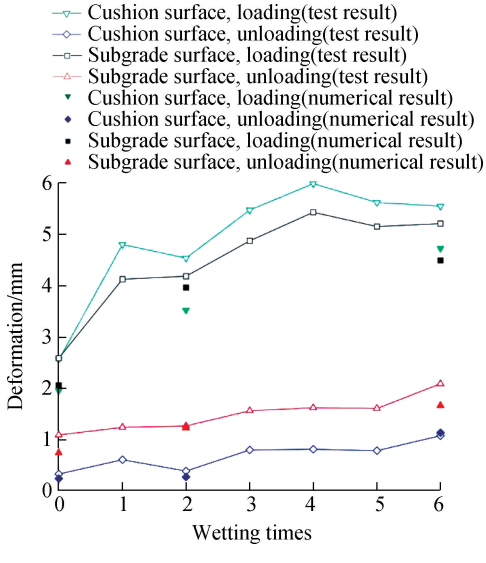

Fig. 2 Result verification of the numerical model

3 Stress Responses of the Cushion under the Boundary Effect

3.1 Numerical simulation

With different thicknesses and elastic moduli of hill-skill stone cushions, as well as different loading widths, the influencing mechanism of the boundary effect was analyzed using the verified numerical models with different model sizes in each numerical condition. The values of the sizes and width of each numerical model are the same in each numerical calculation condition. The composition of the numerical model and the calculation conditions are summarized in Table 4. The initial size of the model is 2.0 m. The size of the model in each calculation condition in Table 4 is changed to 1.6, 2.0, 2.4, 2.8, and 3.2 m. The other parameters in each calculation condition remain unchanged except for model length.

3.2 Boundary effect on the stress responses of the cushion under different loading conditions

The variation coefficient is the ratio of the peak horizontal tensile stress to the initial stress. Fig. 3 shows the evolution characteristics of the variation coefficient of the transverse peak tensile stress (S11) of the cushion with different cushion parameters and model sizes. As shown in Figs. 3(a) and (b), the transverse peak stress decreases

Table 4 Simulation conditions

Condition No.	Thickness of the cushion/m	Elastic modulus of the cushion/MPa	Loading width/m
1	0.15	200	0.45
2	0.20	200	0.45
3	0.25	200	0.45
4	0.30	200	0.45
5	0.25	800	0.45
6	0.25	1 400	0.45
7	0.25	2 000	0.45
8	0.25	200	0.35
9	0.25	200	0.55
10	0.25	200	0.65

as the cushion thickness increases, and the variation rate gradually decreases. However, when the cushion thickness is less than 0.20 m, the reduction rate of the lateral peak stress first decreases and then increases as the model size increases. When the cushion thickness is more than 0.25 m, the boundary effect has only a slight influence on the mechanical response of the cushion. After subgrade wetting, the influence of the boundary effect decreases, and the reduction effect of the thickness of the cushion on the transverse peak stress increases.

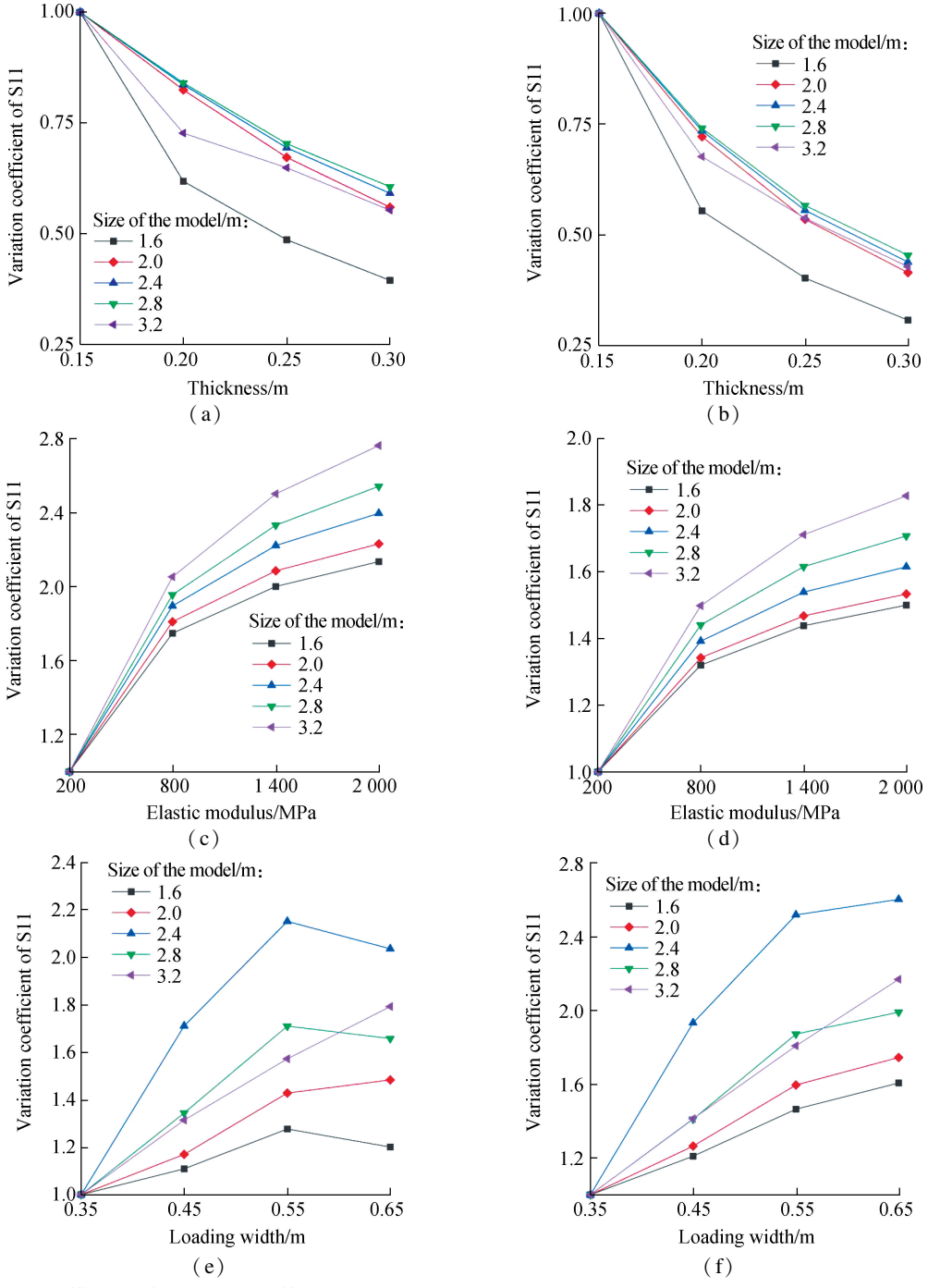

Fig. 3 Variation coefficient of S11 under different cushion parameters. (a) Thickness before subgrade wetting; (b) Thickness after subgrade wetting; (c) Elastic modulus before subgrade wetting; (d) Elastic modulus after subgrade wetting; (e) Loading width before subgrade wetting; (f) Loading width after subgrade wetting

As shown in Figs. 3(c) and (d), with different model sizes, the increase rate of the transverse peak stress gradually decreases with the increase in the cushion elastic modulus. Before subgrade wetting, the increase rate of the transverse peak stress caused by the increase in the cushion elastic modulus is proportional to the model size, which also indicates that the influence of the boundary effect increases. After subgrade wetting, the increase rate of the lateral peak stress caused by the increase in the cushion elastic modulus significantly decreases, and the difference in the variation rate of the lateral peak stress decreases with different model sizes, which indicates that the influence of the boundary effect is reduced.

As shown in Figs. 3(e) and (f), before subgrade wetting and with different model sizes, the increase rate of the lateral peak stress first increases and then decreases with the increase in the loading width by 0.55 m. After subgrade wetting, the variation rate of the lateral peak stress with different loading widths significantly increases. With different model sizes, as the loading width increases, the lateral peak stress shows a two-stage linearly increasing trend, and the increase rate of the lateral peak stress gradually decreases, which indicates that the influence of the boundary effect increases. As the loading width increases from 0.45 to 0.55 m, the increase rate of the lateral peak stress remains constant.

With different model sizes, Fig. 4 shows the evolution

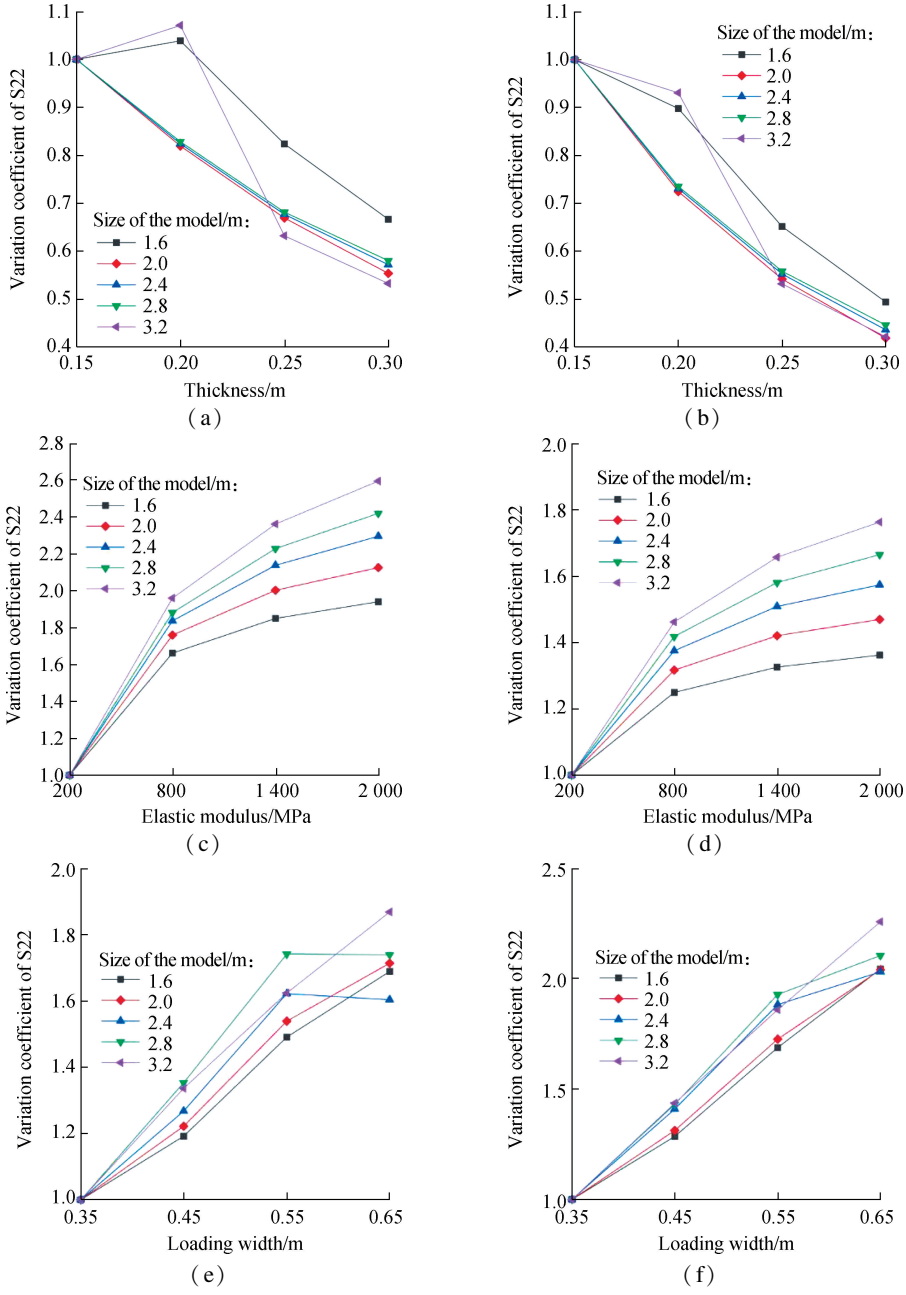

Fig. 4 Variation coefficient of S22 under different cushion parameters. (a) Thickness before subgrade wetting; (b) Thickness after subgrade wetting; (c) Elastic modulus before subgrade wetting; (d) Elastic modulus after subgrade wetting; (e) Loading width before subgrade wetting; (f) Loading width after subgrade wetting

characteristics of the variation coefficient of the longitudinal peak tensile stress (S22) of the cushion with different parameters before and after subgrade wetting. As shown in Figs. 4(a) and (b), the longitudinal stress decreases as the cushion thickness increases. When the model size varies from 2.0 to 2.8 m, the decrease rate of the longitudinal stress caused by the increase in the cushion thickness remains nearly constant. After subgrade wetting, the decrease rate of the peak stress increases, and the decrease rate of the peak stress gradually decreases because of the increase in the cushion thickness. When the cushion thickness is less than 0.25 m, significant differences in the variation characteristics of the longitudinal peak stress can be detected. Before subgrade wetting, the longitudinal peak stress first increases and then linearly decreases with the increase in the cushion thickness. The influence of the boundary effect on the longitudinal peak stress caused by the cushion thickness decreases after subgrade wetting.

As shown in Figs. 4(c) and (d), the evolution characteristics of the longitudinal and transverse peak stresses caused by the cushion elastic modulus are similar even with different model sizes. The larger the model size before and after subgrade wetting, the higher the variation rate of the longitudinal peak stress is. The increase rate of the longitudinal peak stress caused by the increase in the cushion elastic modulus gradually decreases. Within the same range of the cushion elastic modulus, the increase rate of the peak stress induced by the increase in the elastic modulus of the cushion gradually increases with the increase in the model size. The variation rate of the longitudinal peak stress with the elastic modulus of the cushion significantly decreases after subgrade wetting.

As shown in Figs. 4(e) and (f), before and after subgrade wetting, the longitudinal peak stress linearly increases with the increase in the loading width. Before subgrade wetting, when the cushion thickness is more than 0.55 m, with different model sizes, significant differences in the variation characteristics of the longitudinal peak stress with the cushion thickness can be detected. As the loading width increases from 0.45 to 0.55 m, the increase rate of the peak stress caused by the increase in the loading width is stable even with different model sizes. After subgrade wetting, with the increase in the loading width, the longitudinal peak stress linearly increases, and the variation rate significantly increases. When the loading width changes between 0.45 m and 0.55 m, the increase rate of the longitudinal peak stress induced by the increase in the loading width with different model sizes is the same. After subgrade wetting, the variation rate of the longitudinal peak stress with loading width significantly increases under different model sizes, and the difference in the variation rate decreases, which indicates that the influence of the boundary effect decreases.

4 Influence Parameters of the Mechanical Responses of the Cushion with Different Model Sizes

4.1 Principle of gray correlation analysis

The gray correlation analysis method[26] is widely used in the evaluation of the correlation degree or the analysis of the sensitivity of various elements in the system. The method can determine the influence degree of each main factor of the system through strict mathematical matrix operations and quantitatively characterize the sensitivity of each main factor to changes.

4.2 Calculation method of gray correlation analysis

4.2.1 Determination of the incidence matrix

To determine the influence of various experimental variables on the stress response of the cushion, the peak horizontal tensile stress of the cushion is selected as the evaluation indicator. Variables that affect the stress response of the cushion (i.e., thickness, elastic modulus of the cushion, and loading width) are selected as the comparison sequence ($\boldsymbol{X}$), and the stress response indicators of the cushion corresponding to each parameter are used as the reference sequence ($\boldsymbol{Y}$). The specific form of the matrix can be expressed as follows:

$$\boldsymbol{X}=\begin{bmatrix} x_1 \\ x_2 \\ \vdots \\ x_m \end{bmatrix}=\begin{bmatrix} x_{11} & x_{12} & \cdots & x_{1n} \\ x_{21} & x_{22} & \cdots & x_{2n} \\ \vdots & \vdots & & \vdots \\ x_{m1} & x_{m2} & \cdots & x_{mn} \end{bmatrix} \tag{2}$$

$$\boldsymbol{Y}=\begin{bmatrix} y_1 \\ y_2 \\ \vdots \\ y_m \end{bmatrix}=\begin{bmatrix} y_{11} & y_{12} & \cdots & y_{1n} \\ y_{21} & y_{22} & \cdots & y_{2n} \\ \vdots & \vdots & & \vdots \\ y_{m1} & y_{m2} & \cdots & y_{mn} \end{bmatrix} \tag{3}$$

4.2.2 Dimensionless processing of the incidence matrix

Given different data types in the comparison and reference sequences, each datum has different dimensions and numerical values. To avoid computational errors, variation is used as a dimensionless method to process various elements in the matrix, and the following equation is employed for dimensionless processing:

$$x'_{ij}=\frac{x_{ij}-\min x_i}{\max x_i-\min x_i} \tag{4}$$

$$y'_{ij}=\frac{y_{ij}-\min y_i}{\max y_i-\min y_i} \tag{5}$$

4.2.3 Calculation of gray correlation degree

After the dimensionless processing of the incidence matrix, the difference sequence matrix can be obtained by processing the data in the dimensionless matrix as follows:

$$m_{ij} = |x'_{ij} - y'_{ij}| \tag{6}$$

where m_{ij} is the element of the difference sequence matrix.

The correlation coefficients (λ_{ij}) of different experimental variables were calculated using the following equation:

$$\lambda_{ij} = \frac{m_{\min} + \gamma m_{\max}}{m_{ij} + \gamma m_{\max}} \tag{7}$$

where γ is the resolution factor with the value usually taken as 0.5; $m_{\max}$ and $m_{\min}$ are the maximum and minimum elements of the difference sequence matrix, respectively. The correlation degree ranges from 0 to 1, and the sensitivity of the experimental variables is higher when the correlation degree is close to 1. The calculation formula of the correlation degree (P_i) for each influencing factor is expressed as follows:

$$P_i = \frac{\sum_{j=1}^{n} \lambda_{ij}}{n} \tag{8}$$

where P_i reflects the influence degree of each factor.

4.3 Analysis of gray correlation calculation

Fig. 5 shows the sensitivity diagram of the horizontal peak stress of the cushion to different parameters with different model sizes. The correlation of the horizontal stress to the cushion thickness is relatively small with different model sizes. The correlation of the horizontal stress to the cushion elastic modulus is hardly affected by the model size, and the correlation of the horizontal stress to the cushion elastic modulus is nearly the same. The correlation of the horizontal stress to loading width is high with different model sizes. Before subgrade wetting, the maximum difference in the correlation of the horizontal stress to various influencing factors is close to 20% with different model sizes.

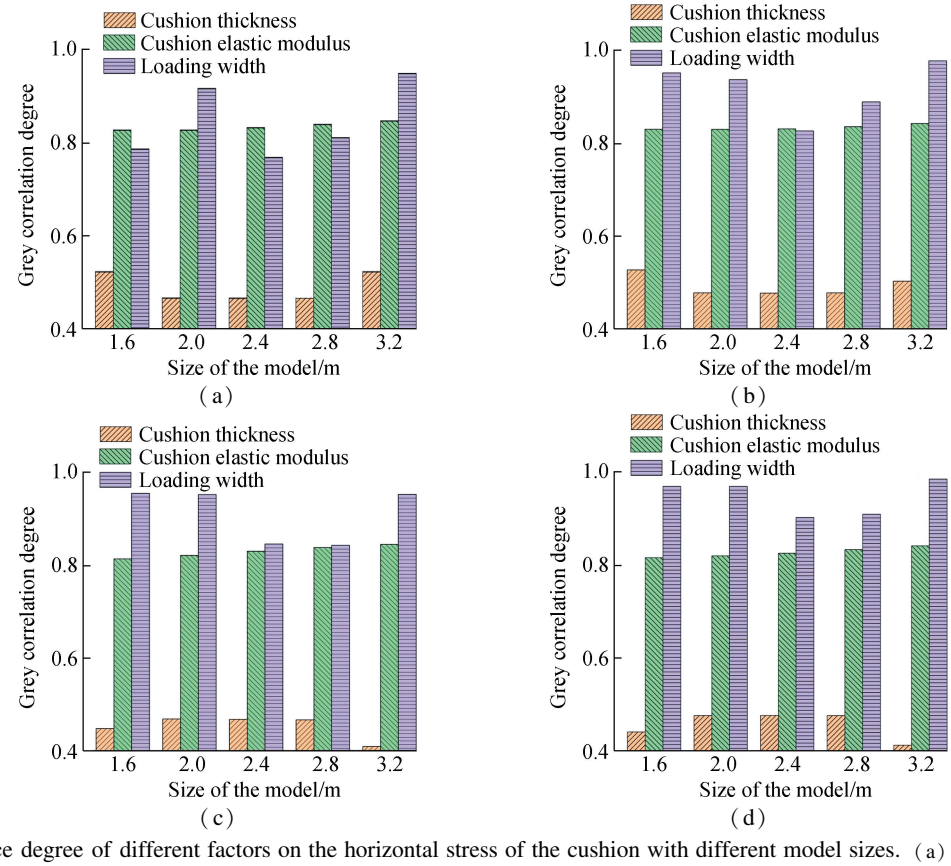

Fig. 5 Influence degree of different factors on the horizontal stress of the cushion with different model sizes. (a) S11 before wetting; (b) S11 after wetting; (c) S22 before wetting; (d) S22 after wetting

After subgrade wetting, the sensitivity of the horizontal peak stress induced by the variation of loading width increases with different model sizes compared with that before subgrade wetting. Meanwhile, the sensitivity of the horizontal stress induced by the change in loading width first decreases and then increases with the increase in the model size. The maximum difference in the correlation of the horizontal stress to various influencing factors is close to 15% with different model sizes, and the difference in the correlation decreases compared with that before subgrade wetting.

5 Conclusions

1) Before subgrade wetting, the horizontal stress of the cushion with different model sizes gradually decreases with the cushion thickness, whereas the decrease rate

gradually decreases. The influence of the boundary effect on the model test can be effectively reduced by the appropriate thickness and elastic modulus of the cushion. After subgrade wetting, the decrease rate of the horizontal stress of the cushion layer increases with the cushion thickness, and the influence of the boundary effects on the stress response of the cushion induced by different cushion thicknesses is reduced.

2) Before subgrade wetting, the horizontal stress of the cushion with different model sizes gradually decreases with the cushion elastic modulus and loading width, whereas the decrease rate gradually decreases. The influence of the boundary effect on the stress response decreases as the cushion elastic modulus increases. After subgrade wetting, the increase rate of the horizontal stress of the cushion with the elastic modulus decreases, whereas the increase rate of the horizontal stress of the cushion with the loading width increases. The influence of the boundary effects on the stress response of the cushion induced by different elastic moduli decreases, and the influence of the boundary effects on the stress response of the cushion induced by different loading widths increases.

3) Before and after subgrade wetting, the sensitivity of the horizontal tensile stress to the change in the cushion elastic modulus remains constant regardless of the model sizes. After subgrade wetting, the sensitivity of the tensile stress to the loading width increases, and the variation of the sensitivity to model size decreases. The research was conducted under static loading. The influence of the boundary effect on model tests under dynamic loading and different types of aircraft loading will be considered in the future.

References

[1] Wang A H, Ding X M, Zhang D W. Grouting reinforcement technology for soft ground differential settlement disease of in-service highway[J]. *Journal of Southeast University* (*Natural Science Edition*), 2017, **47**(2): 397 – 403. DOI: 10.3969/j.issn.1001-0505.2017.02.032. (in Chinese)

[2] Liu W Z, Shi Z G, Zhang D W, et al. Long-term settlement calculation of structured soft clay foundation under traffic loading[J]. *Journal of Southeast University* (*Natural Science Edition*), 2018, **48**(4): 726 – 735. DOI: 10.3969/j.issn.1001-0505.2018.04.020. (in Chinese)

[3] Zhang Y M, Bao F, Tong Z, et al. Radar wave response of slab bottom voids in heterogeneous airport concrete pavement[J]. *Journal of Southeast University* (*Natural Science Edition*), 2023, **53**(1): 137 – 148. DOI: 10.3969/j.issn.1001-0505.2023.01.017. (in Chinese)

[4] Bai M, Liu Z B, Zhang S J, et al. Field test study on moisture adjustment of wicking geotextile in road subgrade[J]. *Journal of Southeast University* (*Natural Science Edition*), 2022, **52**(1): 117 – 123. DOI: 10.3969/j.issn.1001-0505.2022.01.015. (in Chinese)

[5] Liu C X, Tao L J, Bian J, et al. Influence of the liquefied soil layer distribution on the seismic response of rectangular tunnel[J]. *Journal of Southeast University* (*English Edition*), 2018, **34**(2): 259 – 268. DOI: 10.3969/j.issn.1003-7985.2018.02.016.

[6] Luo Q Q, Zhang S, Ye X Y, et al. Investigation on deformation characteristics of wetting silt subgrade under aircraft loading[J]. *Journal of Central South University* (*Science and Technology*), 2021, **52**(7): 2188 – 2199. DOI: 10.11817/j.issn.1672-7207.2021.07.007. (in Chinese)

[7] Zhang S, Teng J, He Z, et al. Canopy effect caused by vapour transfer in covered freezing soils[J]. *Géotechnique*, 2016, **66**(11): 927 – 940. DOI: 10.1680/jgeot.16.P.016.

[8] Luo Q Q, Zhang S, Li Q, et al. Influence of wetting on the stress response of silt subgrade under aircraft loading[J]. *Advanced Engineering Sciences*, 2023, **55**(3): 87 – 99. DOI: 10.15961/j.jsuese.202101249. (in Chinese)

[9] Chen X B, Wang J T, Liu H, et al. Influence of rainfall on skid resistance performance and driving safety conditions of asphalt pavements[J]. *Journal of Southeast University* (*English Edition*), 2019, **35**(4): 482 – 490. DOI: 10.3969/j.issn.1003-7985.2019.04.011.

[10] Wang C Z, Chen F, Xu W S, et al. Operating speed models for curved segments of highways in plateau regions[J]. *Journal of Southeast University* (*English Edition*), 2022, **38**(1): 85 – 91. DOI: 10.3969/j.issn.1003-7985.2022.01.013.

[11] Tan Y L, Zhu B, Cui S. Experimental study on the static load performance of steel-concrete composite external joints after fatigue loading[J]. *Journal of Southeast University* (*English Edition*), 2023, **39**(3): 269 – 276. DOI: 10.3969/j.issn.1003-7985.2023.03.007.

[12] Liao Y D, Wang X, Feng J R, et al. Influence of mineral admixtures on the mechanical property and durability of waste oyster shell mortar[J]. *Journal of Southeast University* (*English Edition*), 2023, **39**(3): 277 – 283. DOI: 10.3969/j.issn.1003-7985.2023.03.008.

[13] Zhang P Y, Xiong L C, Le C H, et al. Comparison analysis of the bearing capacity of rock-shocked piles and sand piles for offshore wind turbines[J]. *Journal of Southeast University* (*English Edition*), 2023, **39**(4): 384 – 392. DOI: 10.3969/j.issn.1003-7985.2023.04.007.

[14] Luo Q Q, Kou J Y, Yi W N, et al. Numerical investigation on deformation of the water-rich silt subsoil under different compaction conditions[J]. *Electronics*, 2024, **13**(3): 520. DOI: 10.3390/electronics13030520.

[15] Chen Y Z, Huang X M. Research on replacement depth of black cotton soil based on cracking behavior of embankment[J]. *Journal of Southeast University* (*English Edition*), 2020, **36**(4): 436 – 443. DOI: 10.3969/j.issn.1003-7985.2020.04.009.

[16] Chen J, Kong Y, Huang X M, et al. Laboratory evaluation of the effect of longitudinal rutting on transversal permeability in porous asphalt pavement[J]. *Journal of Southeast University* (*Natural Science Edition*), 2016, **46**(3): 584 – 588. DOI: 10.3969/j.issn.1001-0505.2016.03.021. (in Chinese)

[17] Li J, Li Y Y, Xin C S, et al. Dynamic strain response of hot-recycled asphalt pavement under dual-axle accelerated loading conditions[J]. *Coatings*, 2022, **12**(6), 843. DOI: 10.3390/coatings12060843.
[18] Zhang Y. *Analysis on the bottom strain of the layered structure based on the model test*[D]. Xi'an: Chang'an University, 2014. (in Chinese)
[19] Cao H Y, Liu Y F, Li Y N. Size effect of scale models for layered subgrades based on soil's vibration energy absorption characteristics[J]. *Journal of Vibration and Shock*, 2018, **37**(1): 77 - 84. DOI: 10.13465/j.cnki.jvs.2018.01.013. (in Chinese)
[20] Kuo C M, Lin C C, Huang C H, et al. Issues in simulating falling weight deflectometer test on concrete pavements[J]. *KSCE Journal of Civil Engineering*, 2016, **20**(2): 702 - 708. DOI: 10.1007/s12205-015-0299-y.
[21] Miah M T, Oh E, Chai G, et al. Effect of swelling soil on pavement condition index of airport runway pavement [J]. *Transportation Research Record*, 2022, **2676**(10): 553 - 569. DOI: 10.1177/03611981221090517.
[22] Zhang W Z, Xu B S, Zeng Z Y, et al. Research on failure evolution process of surrounding rock of swelling loess tunnel under rainfall infiltration[J]. *Journal of Southeast University (Natural Science Edition)*, 2018, **48**(4): 736 - 744. DOI: 10.3969/j.issn.1001-0505.2018.04.021. (in Chinese)
[23] China Airport Construction Group Corporation. Specifications for airport cement concrete pavement design: MHT/5004—2010 [S]. Beijing: Civil Aviation Administration of China, 2010. (in Chinese)
[24] Luo Q Q, Ye X Y, Li Q, et al. Experimental and numerical study on response characteristics of airport pavement subjected to wetting in silt subgrade[J]. *KSCE Journal of Civil Engineering*, 2023, **27**(2): 551 - 566. DOI: 10.1007/s12205-022-0647-7.
[25] Ministry of housing and urban rural development of the People's Republic of China. Code for design of building foundation: GB 50007—2011 [S]. Beijing: Architecture and Building Press, 2011. (in Chinese)
[26] Xu L P, Ma H Y, Ren D Z. Reliability analysis of tractor multi-way valves based on the improved weighted grey relational method[J]. *The Journal of Engineering*, 2019, **2019**(13): 86 - 92. DOI: 10.1049/joe.2018.8985.

粉土湿化作用下边界效应对垫层力学响应试验的影响

罗其奇[1] 余 虔[2] 张 升[1] 马新岩[1,2] 叶新宇[1,3] 杜银飞[1,3]

([1] 中南大学土木工程学院,长沙 410075)
([2] 民航机场规划设计研究总院有限公司岩土工程所,北京 100020)
([3] 湖南铁院土木工程检测有限公司,长沙 410075)

摘要:采用自研的模型试验系统,研究了道基湿化过程中粉土力学特性和机场跑道变形特征.依据试验结果验证了数值模拟结果的可靠性,并建立了不同尺寸的数值模型.在相同垫层参数和荷载宽度区间条件下,研究了道基湿化前后边界效应对垫层力学响应的影响.结果表明,不同湿化程度粉土内摩擦角接近34°,黏聚力为8~44 kPa,弹性模量为15~34 MPa.道基湿化前后,受边界效应影响,相同垫层参数和荷载宽度区间下垫层水平拉应力的变化率并不相同.道基湿化后,相同垫层参数区间下垫层水平拉应力变化率差异较湿化前减小,相同荷载宽度区间下变化率差异却有所增加.道基湿化前后边界效应对垫层应力响应评估的影响不利于道面设计参数优化.垫层厚度大于0.25 m时,可忽略边界效应的影响.

关键词:道面垫层;粉土道基;湿化;边界效应;力学响应
中图分类号:U416.2